Turkish Journal of Electrical Engineering & Computer Sciences

http://journals.tubitak.gov.tr/elektrik/

Research Article

Turk J Elec Eng & Comp Sci
(2016) 24: 2042 – 2052

doi:10.3906/elk-1304-80

Design of a frequency control system in a microgrid containing HVAC

Mohammad KOOCHAKIAN JAZI*, Seyed Masoud MOGHADDAS TAFRESHI, Mehdi JAFARI
Faculty of Electrical Engineering, K.N.Toosi University of Technology, Tehran, Iran

Received: 09.04.2013 • **Accepted/Published Online:** 29.06.2014 • **Final Version:** 15.04.2016

Abstract: The advent of smart grids and the growing procedure of controllable loads and tending to the demand response (DR) in small power systems have helped with new ideas, which can be used in the frequency stability of a microgrid. This paper presents a novel model for frequency control of a microgrid containing controllable load and renewable resources. The controllable loads used in this paper are such as heating, ventilation, and air conditioning, which change temperature based on frequency change. The microgrid is hybrid (AC/DC) and able to connect to and energy exchange with the utility grid. The design of PID controller parameters is considered an optimization problem according to the time domain-based objective function solved by the particle swarm optimization (PSO) algorithm, which has a strong ability to find the most optimistic results. The effectiveness and robustness of the proposed controller are demonstrated through nonlinear time-domain simulation. Finally, for the simulation and analysis, the output results have been presented and studied.

Key words: Controllable load, frequency control, PID control, microgrid

1. Introduction

The paradigm change toward sustainable electricity has led to the development of renewable resources. Hence, fluctuations in the power system increased significantly with the growth of renewable resources. The grid frequency must be controlled within acceptable limits; otherwise it will lead to instability and the grid may even collapse. In recent years, demand for renewable resources especially wind and PV facilities is growing. Frequency stability has become more important in microgrids due to changes in climate and changes in consumption by consumers [1]. In [2] without real-time information and in [3] a statistical model of a heating system of heater pump have been used to control frequency. [4,5] have used an electrical water pump and electrical vehicles to control frequency and voltage in a small power grid and islanded grid, respectively. The reference [6] has used flywheel frequency control.

In [7] frequency controls were conducted by an aggregator using the predictive-control approach. One of the most important features of a smart grid is to have an advanced structure that can facilitate the connection of various AC and DC generation systems, energy storage options, and DC [8] and AC loads with optimized operation. In a smart grid, the power of the demand side can also be used in order to balance the production and consumption and participate in frequency control [9]. Hence, controllable loads can be used to balance the consumption and production and to be utilized in the stability of the system frequency.

In this paper, frequency control of a microgrid is conducted by heating, ventilation and air conditioning

*Correspondence: koochakian.jazi@gmail.com

(HVAC) as controllable load. The HVAC increases its efficiency due to having a hybrid (AC/DC) structure and increases its ability of connecting to and energy exchanging with the utility grid because it can feed the AC and DC loads concurrently. AC sources and loads are tied to the AC bus, whereas dc sources and loads are connected to the DC bus. The microgrid can operate in a grid-tied or islanded mode and connect to the utility grid by AC link. Considering the inertia system, the HVAC participates in the frequency stability and balancing the demand side. In order to control frequency in the proposed microgrid, the PID control structure is used due to having a derivative component that has better ability than the PI controller [10] in transient stability. Heuristic methods for solving problems in the best approach are optimization of complex problems [11]. For this reason, PSO is used for optimizing. The results of simulation in MATLAB software are also presented and evaluated.

The paper is organized in the following way. First, the proposed microgrid structure and its components are presented in Section 2. Then the microgrid control structure is described in Section 3 and the results of the simulation are given in Section 4. Section 5 provides the conclusion.

2. Modeling of the proposed structure of the microgrid and its components

2.1. The structure of the proposed hybrid microgrid

The proposed structure of the microgrid is presented in Figure 1.

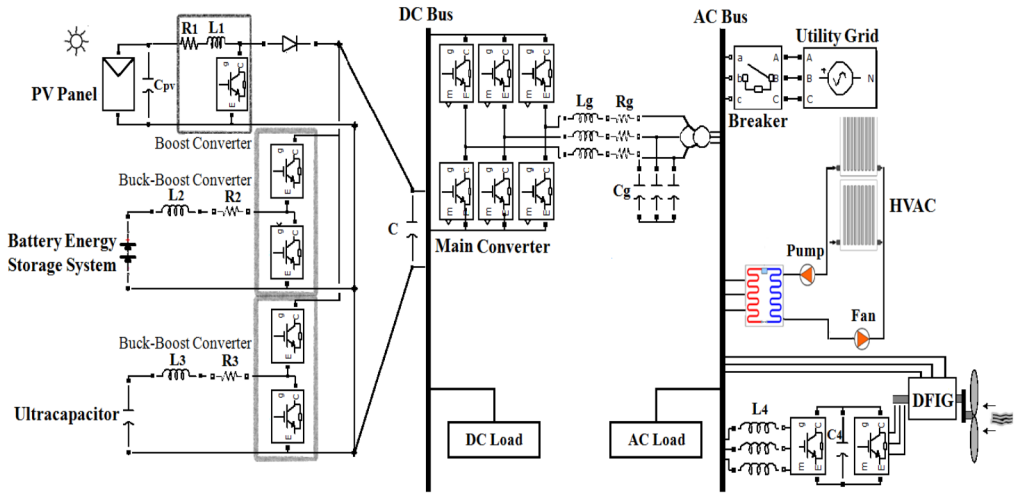

Figure 1. Proposed hybrid microgrid structure.

As seen in Figure 1, a PV module with a nominal value of 50 kw and a 50 kw wind turbine generator (WTG) with the type of doubly fed induction generator (DFIG) technology are connected to the DC and AC links by a boost converter, respectively. A capacitor C_{pv} is to restrain high frequency ripples of the PV output voltage. To keep the energy of the microgrid in a steady state, a battery with nominal values of 200 v, 65 ah, and SOC 40% and an ultracapacitor with nominal values of 6.5 f and 350 v for rapid response to high volatility have been used and connected to DC bus by using a DC/DC buck-boost converter. The proposed microgrid is connected to the utility grid through an AC bus and it operate in both parallel and island modes as well as having the ability to feed AC and DC loads with variable values (10 kw–50 kw) concurrently. AC and DC loads in the microgrid are connected to the AC and DC links. The connected DC load includes pure resistive

load and the connected AC load including constant impedance load (resistor - inductor) and a fixed capacitor. The rated voltages for the DC and AC buses are 400 v and 400 v rms, respectively. A three-phase inverter that can transfer electrical power in both directions connects to the DC bus with an R-L-C filter and an isolation transformer. As can be seen, the HVAC is connected to the AC bus as controllable load.

2.2. Modeling energy sources

2.2.1. Wind turbine generator

The DFIG system has capability of voltage and frequency adjustment using the rotor current control independently. The basic configuration of the DFIG and WTG is explained in [12].

2.2.2. PV panel

The equivalent circuit of a PV panel is a controllable current source whose relations and parameters are shown in [10].

2.2.3. Energy storage system

Although the use of renewable resources has significant advantages, it does not have appropriate reliability. Therefore, an energy storage system has been used to enhance system reliability. The system is composed of the following two parts.

2.2.3.1. Ultracapacitor

Ultracapacitors are electrolytic devices with high capacity that store energy in the form of an electrostatic charge. The ultracapacitor can have very high discharge rates and can track changes in the microgrid quickly. The ultracapacitor circuit model based on an energy storage system is explained in [13].

2.2.3.2. Battery

The battery is modeled as a nonlinear voltage source whose output voltage depends on not only current but also on the SOC. The battery model is a nonlinear function dependent on time and current as explained in [10].

2.2.4. HVAC system

The main purpose of this system is the air conditioning of the building. In this paper, the HVAC system is used to control the frequency of the microgrid. This system is equipped with a dynamic control system that it is sensitive to the production and consumption of the microgrid. The system maintains the consumer's comfort level as well as temperature control. The following method is used to implement the model.

First, the consumer chooses a temperature as the desired temperature ($T_{Desired}$). Then the controller according to the desired temperature will act to ensure the consumer's comfort level and building temperature range is maintained between 20 and 26 °C.

The HVAC's controllable load operates based on demand supply balancing process according to the restriction on the consumer's comfort level of the HVAC in the microgrid. The HVAC's performance is described in the flowchart in Figure 2. If the HVAC is able to balance the power, Eqs. (1) and (2) will be established; otherwise the surplus power be compensated by controllers of the microgrid.

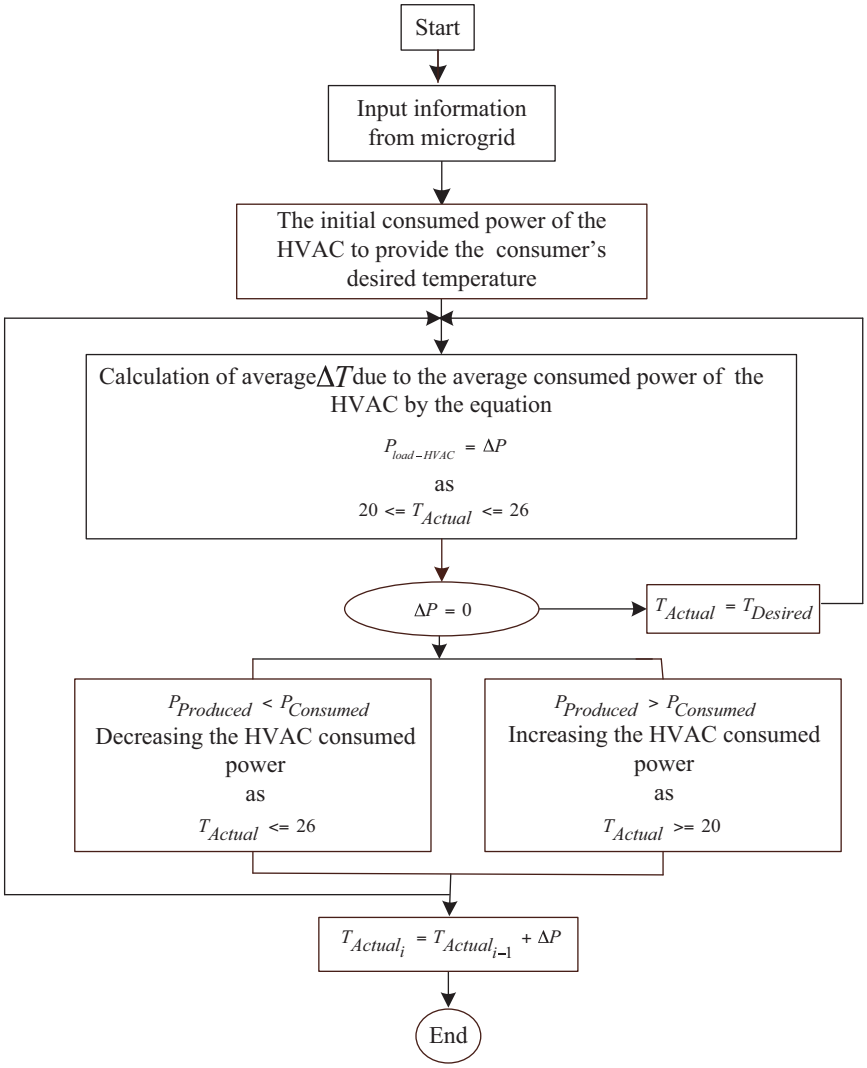

Figure 2. Flowchart for calculating ΔT and HVAC power for frequency stability.

$$\Delta P = (\pm\ P_{Grid}[1] + P_{wind}[2] + P_{pv}[3] \pm P_{uc}[4] \pm P_{bat}[5])(-(P_{Load-AC}[6] + P_{Load-DC}[7])\ P_{Load-HVAC}[8] = \Delta P$$

According to the flowchart in Figure 2, first it is assumed that the HVAC system acts as a cooler, and then the consumer sets his/her $T_{Desired}$ and a power will be spent to meet the desired temperature by the HVAC. Now, if the mentioned temperature range is established, the controller will act in a way that Eq. (2) is fulfilled. Otherwise, creating equality the other microgrid components such as energy storages are used.

The consumed power of the HVAC is according to temperature change ΔT in the environment. ΔT is the temperature difference created by the HVAC's cooling system at the time interval. In order to make a temperature difference, it is sufficient that equivalent energy is used by the energy equation (3), where ρ_{air} is

[1]The power exchange with utility grid
[2]The produced power by wind resource
[3]The produced power by PV panel
[4]The produced (consumed) power by discharged (charged) ultracapacitor
[5]The produced (consumed) power by discharged (charged) battery
[6]The consumed power AC load
[7]The consumed power DC load
[8]The consumed power HVAC load

density of air (g/m^3) with the value of 1.18e^{-3} and V$_{room}$ is the volume of space (m^3) with the value of 1.012.

$$P_{Load-HVAC} \times t \times SEER - Q_{Leak} = -\rho_{air}.V_{room}c_{air}.\Delta T$$

In this paper, the value of seasonal energy efficiency ratio (SEER) [14] is considered 10. Q$_{Leak}$ is thermal energy exchange between internal and external space; so the heat transfer rate depends on the inside ambient temperature and outside ambient temperature and is obtained by Eq. (4).

$$H = kA\frac{T_{out} - T_{in}}{L}$$

H is heat flow rate from outside to inside atmosphere, k is the thermal conductivity (w/mk), A is the area of a wall (m^2), L is wall thickness (m), T$_{out}$ is outside temperature, and T$_{in}$ is inside temperature (k).

2.3. Control strategy in the proposed microgrid

2.3.1. Parallel operation

PV panel

When the solar unit is in this mode, the control converter is placed at maximum power point tracking (MPPT). To achieve this objective, the P&O algorithm [15] is used.

2.3.1.2. Control of DFIG

The DFIG control block includes the rotor-side converter and grid-side converter. The control block diagram model in [12] is given.

2.3.1.3. Modelling and control of the main converter

The frequency and voltage adjustment will be realized in a d–q rotating system by inverter in the form of power division dynamically. To exchange power between the AC and DC links is the important role of the main converter. The converter operates in the two modes and provides active and reactive power requirements according to grid conditions.

As mentioned, first the microgrid active and reactive currents are obtained and then they are transferred to the d–q rotating system. The voltage of the DC bus is obtained by reference active moment current (i$_d$) and reference reactive moment current (i$_q$) of the inverter through the PID controller. Then it is passed through the PID controller after that comparing to the current obtained from the inverter. In this case, voltage of i$_d$ and i$_q$ is compared to the grid-side voltage and the voltage of the inverter, which is obtained by multiplying inverter current by the ωL$_g$ as shown in Figure 3, and a suitable command is given to the PWM.

2.3.1.4. Hybrid battery and ultracapacitor energy storage system

The battery has a high energy density, while it has a low charge and discharge rate. On the other hand, the ultracapacitor has a high power density and high speed in response. The energy storage units can be combined and complement each other. According to these characteristics, the control structure of the hybrid energy storage is proposed in Figure 4. Therefore, the high frequency disturbance and the low frequency disturbance are destroyed by the ultracapacitor and battery in the DC link, respectively. Cut-off frequency of the low-pass filter (LPF) is 25 Hz.

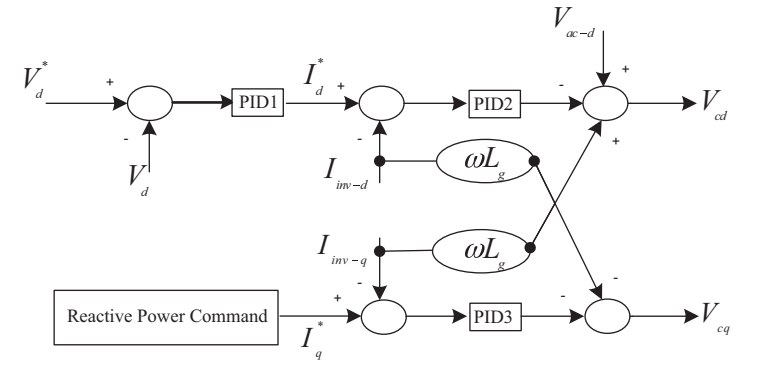

Figure 3. PQ control structure of the main converter.

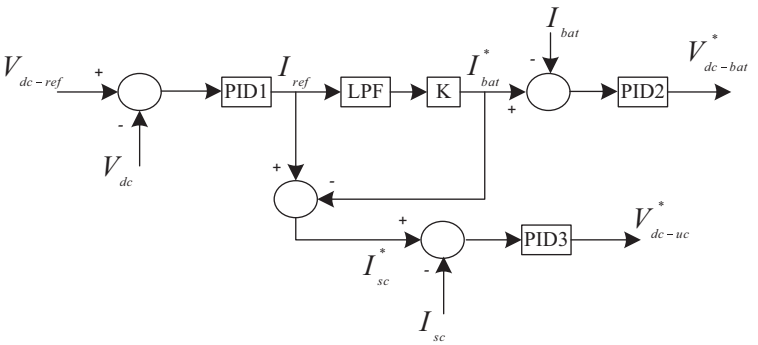

Figure 4. Control structure hybrid battery and ultracapacitor.

2.3.2. Islanded operation

The microgrid operates in islanded mode when a fault occurs in the utility grid. In this mode, most controllers will behave as before. As mentioned previously, controllable load participates based on its sensitivity to the grid and the consumer's comfort level in frequency stability, but it may not be able to remove oscillation of frequency. Therefore, the main converter also plays a role in eliminating fluctuations. In the islanded mode, the main converter controls AC bus voltage [16] and destroys another part of the frequency oscillation and ensures appropriate frequency stability finally. Figure 5 shows the control structure in the islanded mode.

3. The strategy of PSO algorithm for solving problem

In order to optimize the controller parameters, the PSO optimization algorithm [17] is used. In this paper, the solution is based on Eq. (5).

This fitness function was mathematically defined as follows:

$$E = E_f + E_{vAC} + E_{vDC}$$

Each of which includes:

$$E_f = \sum_{t_s} t \times \| f_{AC-measured}(t) - f_{AC-ref}(50Hz) \|$$

$$E_{vAC} = 0.01 \times \sum_{t_s} t \times \left\| \begin{array}{l} v_{AC-measured}(t) \\ -v_{AC-ref}(400Vrms) \end{array} \right\|$$

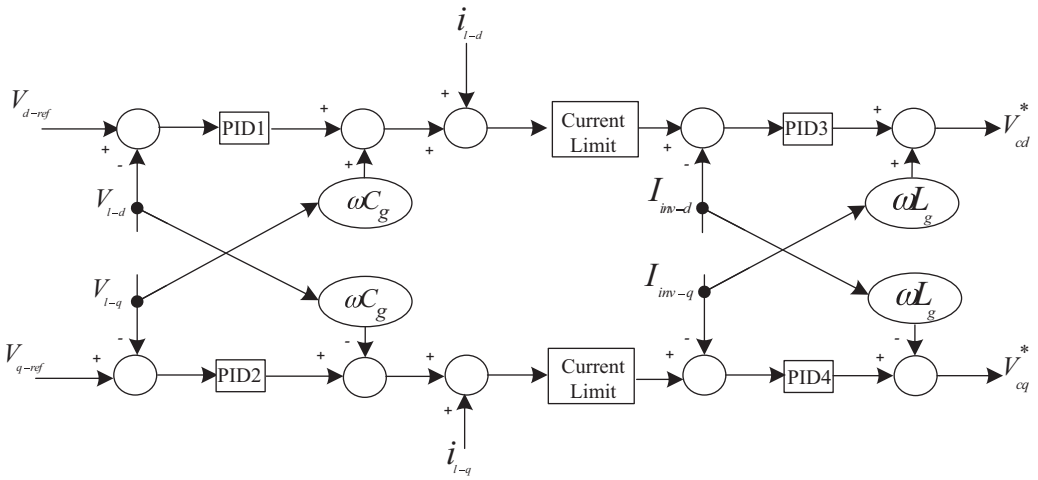

Figure 5. Control block diagram of the main converters in islanded mode.

$$E_{vDC} = 0.01 \times \sum_{t_s} t \times \left\| \begin{array}{c} v_{DC-measured}(t) \\ -v_{DC-ref}(400V) \end{array} \right\|,$$

where t_s is simulation time, and $f_{AC-measured}$, $v_{AC-measured}$, and $v_{DC-measured}$ are measured frequency of the AC bus, and measured voltage of the AC and DC buses, respectively. F_{AC-ref}, v_{AC-ref}, and v_{DC-ref} are reference frequency and reference voltages of the AC and DC buses, respectively.

4. Dynamic simulation

In this section, after finding the optimal controllers gain by PSO, simulation results are presented and the parameters used in the proposed microgrid are presented in the Table. First in case (a), it is assumed that during simulation, the wind speed and the solar radiation level are fixed and equal to 10 m/s and 1000 w/m^2, respectively, and also the consumer's desired temperature is 23 °C.

The overall consumed power in microgrid are the AC inductive load with the value of 25 kw, the induction motor with the value of 7.5 kw and the DC load with the value of 16 kw. ΔP is the difference between the microgrid produced and consumed power. According to Figures 6 and 7, when the microgrid is connected to the utility grid, its AC voltage and frequency will be equal to the utility grid AC voltage and frequency. However, when an error occurs in the utility grid, the microgrid operates in the isolated mode.

In this paper it is assumed to occur at 0.5 s. The difference between produced and consumed power of the microgrid has the average value of 2867.55 w from 0 to 0.5 s, and it is deduced that before the occurrence of the error, the active power is injected from the utility grid to the microgrid and after being separated from the utility grid, the microgrid frequency falls slightly.

The required reactive power of the microgrid is provided by the utility grid at time t $<$ 0.5 s. The microgrid is lacking reactive power at the time t $>$ 0.5 s (islanded mode). As is known, reactive power flow in turn will affect the voltage drop directly. The simulation's results shown in Figure 7 demonstrate this. The voltage drop at t = 0.5^+ s is equal to 152 v (Figure 7). At this time, amounts of storage capacity are used to compensate for the shortage of reactive power.

Table. Suggested parameters for the microgrid.

Value	Description	Symbol
0.12 f	Capacitor across the DC-link	C
0.7 Ω	Filtering resistance for the inverter	R_g
1.2 mh	Filtering inductor for the inverter	L_g
$200e^{-6}$ f	Filtering capacitor for the inverter	C_g
$110e^{-6}$ f	Capacitor across the PV panel	C_{pv}
$25e^{-4}$ h	Inductor for PV boost converter	L_1
$1e^{-12}\Omega$	Resistance for PV boost converter	R_1
0.0006 h	Inductor for battery buck-boost converter	L_2
0.03 Ω	Resistance for battery buck-boost converter	R_2
0.0006 h	Inductor for ultracapacitor buck-boost converter	L_3
0.77 Ω	Resistance for ultracapacitor buck-boost converter	R_3
12 khz	Switching frequency of power converter	f_s
36° c	Outside temperature	T_{out}
400 m^3	Volume of space	V_{room}
24 m^2	Area of a wall	A
0.1 w/mk	Thermal conductivity	K
50 hz	Frequency of the AC grid	F
400 v	Rated DC bus voltage	V_{DC}
400 v	Rated AC bus voltage	V_{AC-rms}

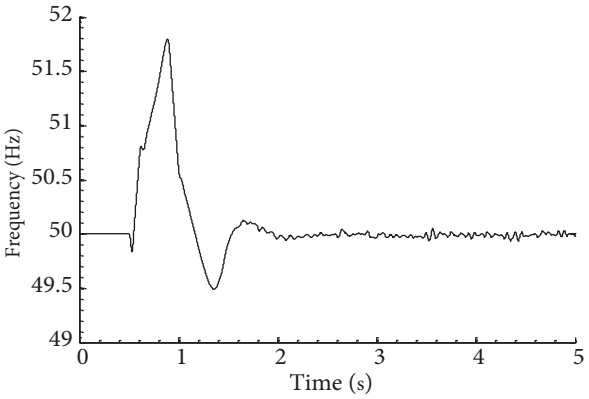

Figure 6. The proposed microgrid frequency in islanded mode in case (a).

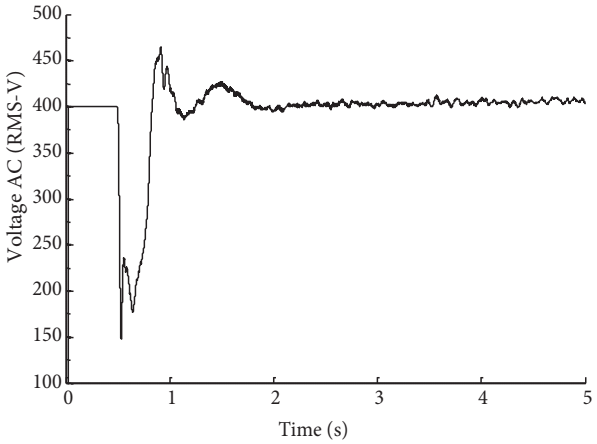

Figure 7. The proposed microgrid AC voltage in islanded mode in case (a).

The battery and ultracapacitor would be charged and discharged in the microgrid, in a way that the DC voltage remains constant to its desired value (400 v) in accordance with Figure 8. According to the flowchart in Figure 2, the HVAC receives data from the power differences and then it controls the consumed power if the consumer's comfort level is not disrupted and the building temperature does not exceed 20–26 °C.

To eliminate high-frequency oscillations in the DC link, a capacitor with the value of 0.12 f is used. In the process of simulation, the capacitor is charged at t = 0.0^+ s, which causes DC voltage equal to 200 v at this time but it increases to 400 v after a short time.

As seen in Figure 9, before the microgrid is separated from the utility grid, the HVAC consumes power in order to reach the desired temperature, which is decreased before 0.5 s slightly. Now, after the microgrid is

separated from the utility grid, it can be seen that the amount of consumed power has increased by the HVAC. One of the reasons is the discharge of the ultracapacitor and battery so that on one hand the production and the frequency increase in value and on the other hand the desired DC voltage level is achieved. Moreover, the power balance is observed by microgrid ingredients averagely and the secondary and tertiary frequencies are in the allowed range. The changes in the average temperature of the building at steps i = 0.5 s are shown in Figure 10.

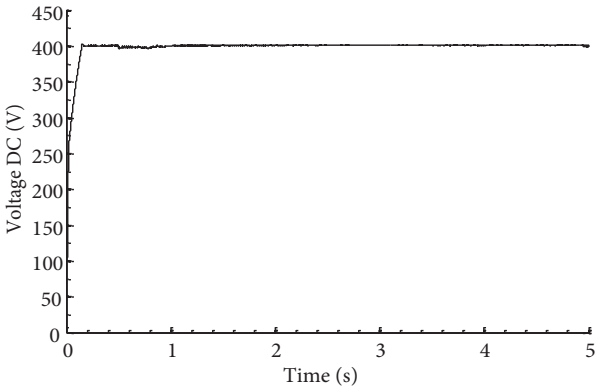

Figure 8. The proposed microgrid DC voltage in islanded mode in case (a).

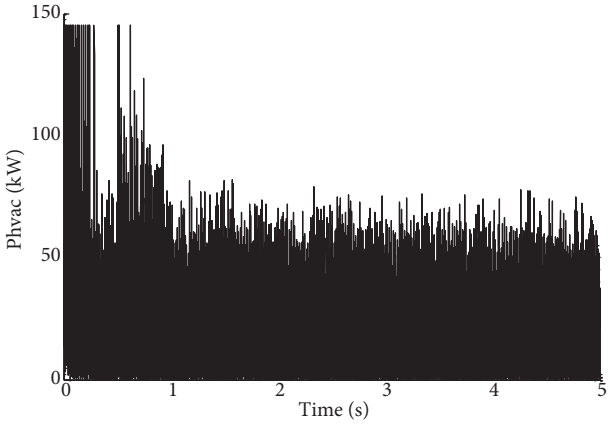

Figure 9. Amount of consumed power by the HVAC in case (a).

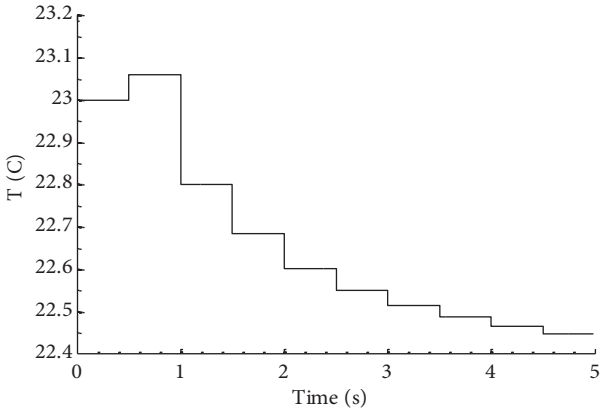

Figure 10. Average temperature in the building in case (a).

In case (b), it is assumed that wind speed changes from 10 m/s to 8 m/s and the solar radiation level changes according to Figure 11; moreover, the AC consumed load will be increased during 2 to 2.5 s to the amount of 20 kw concurrently. In this case, with the constant desired temperature, the following results are achieved.

In Figure 12, as can be seen, the secondary oscillation frequency compared to (a) increases, but it is quickly damped.

With the increase in wind speed in case (b), the wind power increases, and then the average consumed power of the HVAC will increase (Figure 13). Changing the solar radiation level makes the DC voltage level change and also ultracapacitor and battery are discharged immediately.

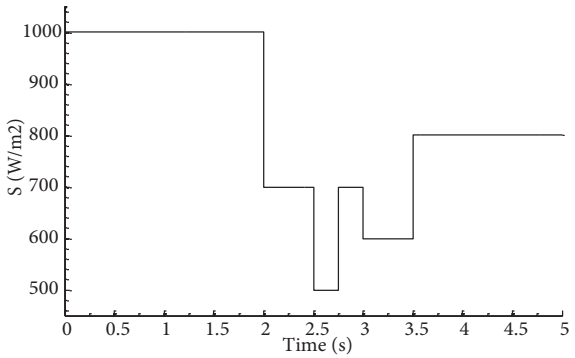

Figure 11. The solar radiation level changes in case (b).

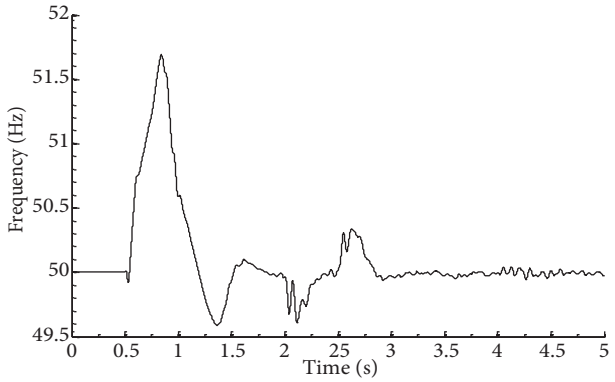

Figure 12. The proposed microgrid frequency in islanded mode in case (b).

When AC load increases at 2 to 2.5 s, the transfer power and produced power in the AC-side bus decrease from the DC bus to the AC bus and so the AC-side frequency and voltage (Figure 14) are reduced. In addition, as can be seen in Figure 13, the average consumed power is reduced by the HVAC at 2 to 2.5 s and reaches the value of 14424.02 w compared to the case in which it does not have the load increasing (17782.26 w); it decreases to 18.88%. AC load change is also effective on the transfer power and the DC bus voltage reduction. However, in this case, the reduction is compensated for by the ultracapacitor and battery.

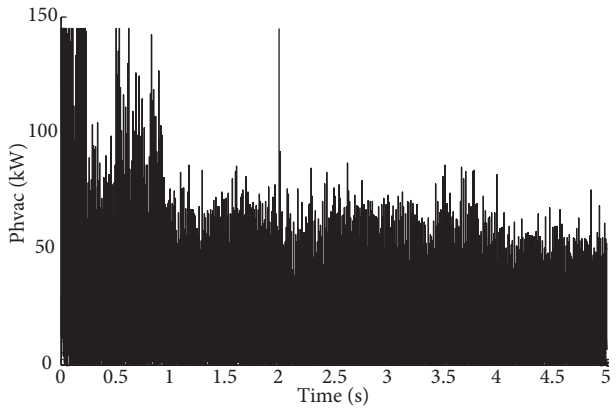

Figure 13. Amount of consumed power by the HVAC in case (b).

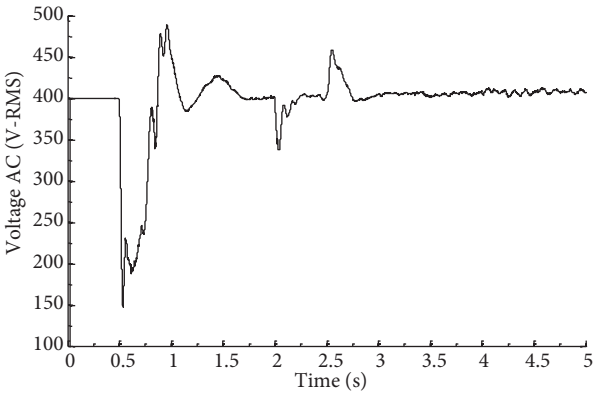

Figure 14. The proposed microgrid AC voltage in islanded mode in case (b).

5. Conclusion

In this paper, a hybrid AC/DC microgrid has been presented including controllable load HVAC with the ability to connect to and exchange energy with the utility grid. The simulation results show that the HVAC participates in the frequency stability while the consumer's desired temperature of the HVAC is fulfilled. Among advantages of this method is that the HVAC operates in a way to ensure an appropriate frequency stability and does not disrupt the consumer's comfort level according to the microgrid's produced and consumed power. This method should be trying to prevent charging and discharging of the battery and supercapacitor constantly to avoid reducing their life.

Acknowledgement

We acknowledge Dr Fariborz Sharifian Jazi for good advice about this paper.

References

[1] Rattanapornchai C, Ngamroo I, Vachirasricirikul S. Robust frequency control in the smart microgrid by heat pump and plug-in hybrid electric vehicle. In: IEEE 2010 Asia PES Proceedings of the IASTED; 24–26 Nov 2010; Phuket, Thailand: IEEE. pp. 146-701.

[2] Masuta T, Yokoyama A. Supplementary load frequency control by use of a number of both electric vehicles and heat pump water heaters. IEEE T Smart Grid 2012; 3: 1253-1262.

[3] Masuta T, Yokoyama A, Tada Y. System frequency control by heat pump water heaters (HPWHs) on customer side based on statistical HPWH model in power system with a large penetration of renewable energy sources. In: IEEE 2010 International Conference on Power System Technology; 24–28 Oct. 2010; Tokyo, Japan: IEEE. pp. 1-7.

[4] Tokudome M, Senjyu T, Yona A, Funabashi T. Frequency and voltage control of isolated island power systems by decentralized controllable loads. In: IEEE 2009 Transmission & Distribution Conference; 26–30 Oct. 2009; Nishihara, Japan: IEEE. pp. 1-4.

[5] Egashira R, Tsuji T, Oyama T, Hashiguchi T, Goda T, Gotou E, Yarimitsu T. A study of system frequency control of island power network using disturbance observer with adaptive behavior controller. In: 2009 ICEE International Conference; 5–9 July 2009; Shenyang, China: ICEE. pp. 1-5.

[6] Takahashi R, Tamura J. Frequency control of isolated power system with wind farm by using flywheel energy storage system. In: IEEE 2008 Electrical Machines 18th International Conference; 6–9 Sept. 2008; Kitami, Japan: IEEE. pp. 1-6.

[7] Galus MD, Koch S, Andersson G. Provision of load frequency control by PHEVs, controllable loads, and a cogeneration unit. IEEE T Ind Electron 2011; 58: 4568-4582.

[8] Tanaka K, Yoza A, Ogimi K, Yona A, Senjyu T, Funabashi T, Kim CH. Optimal operation of DC smart house system by controllable loads based on smart grid topology. Renew Energ 2012; 39: 132-139.

[9] Xu Z, Østergaard J, Togeby M. Demand as frequency controlled reserve. IEEE T Power Syst 2011; 26: 1062-1071.

[10] Liu X, Wang P, Loh PC. A hybrid AC/DC microgrid and its coordination control. IEEE T Smart Grid 2011; 2: 278-286.

[11] RezaieEstabragh M, Mohammadian M, Shafiee M. A novel approach for optimal allocation of distributed generations based on static voltage stability margin. Turk J Elec Eng & Comp Sci 2012; 20: 1044-1062.

[12] Yang L, Xu Z, Østergaard J, Dong ZY, Wong KP, Ma X. Oscillatory stability and eigenvalue sensitivity analysis of a DFIG wind turbine system. IEEE T Energy Convers 2011; 26: 328-339.

[13] Sirmelis U, Grigans L, Latkovskis L. An analytic simulation model for a supercapacitor-based energy storage system. In: IEEE 2011 Proceedings of the European Conference; 30 Aug.–1 Sept. 2011; Riga, Latvia: IEEE. pp. 1-10.

[14] ANSI/AHRI Standard 210/240. Performance rating of unitary air-conditioning & air-source heat pump equipment. USA, June 2011.

[15] Chun WN, Zuo S, Yukita K, Goto Y, Ichiyanagi K. Research of PV model and MPPT methods in MATLAB. In: IEEE 2010 Power and Energy Engineering Conference; 28–31 March 2010; Nanjing, China: IEEE. pp. 1-4.

[16] Marwali MN, Keyhani A. Control of distributed generation systems-part I: voltages and currents control. IEEE T Power Electron 2004; 19: 1541-1550.

[17] Bonabeau E, Dorigo M, Theraulaz G. Swarm intelligence: from natural to artificial systems. IEEE T Evol Comput 2000; 4: 192-193.